Radiative absorption enhancements by black carbon controlled by particle-to-particle heterogeneity in composition

Laura Fierce[a,1], Timothy B. Onasch[b,c], Christopher D. Cappa[d], Claudio Mazzoleni[e], Swarup China[f], Janarjan Bhandari[e], Paul Davidovits[c], D. Al Fischer[g,2], Taylor Helgestad[d,3], Andrew T. Lambe[b], Arthur J. Sedlacek III[a], Geoffrey D. Smith[g], and Lindsay Wolff[c]

[a]Department of Environmental and Climate Sciences, Brookhaven National Laboratory, Upton, NY 11961; [b]Center for Aerosol and Cloud Chemistry, Aerodyne Research, Inc., Billerica, MA 02467; [c]Department of Chemistry, Boston College, Chestnut Hill, MA 01821; [d]Department of Civil and Environmental Engineering, University of California, Davis, CA 95616; [e]Department of Physics and Atmospheric Sciences Program, Michigan Technological University, Houghton, MI 49931; [f]Environmental Molecular Sciences Laboratory, Pacific Northwest National Laboratory, Richland, WA 99352; and [g]Department of Chemistry, University of Georgia, Athens, GA 30602

Edited by Ravi R. Ravishankara, Colorado State University, Fort Collins, CO, and approved January 27, 2020 (received for review November 9, 2019)

Black carbon (BC) absorbs solar radiation, leading to a strong but uncertain warming effect on climate. A key challenge in modeling and quantifying BC's radiative effect on climate is predicting enhancements in light absorption that result from internal mixing between BC and other aerosol components. Modeling and laboratory studies show that BC, when mixed with other aerosol components, absorbs more strongly than pure, uncoated BC; however, some ambient observations suggest more variable and weaker absorption enhancement. We show that the lower-than-expected enhancements in ambient measurements result from a combination of two factors. First, the often used spherical, concentric core-shell approximation generally overestimates the absorption by BC. Second, and more importantly, inadequate consideration of heterogeneity in particle-to-particle composition engenders substantial overestimation in absorption by the total particle population, with greater heterogeneity associated with larger model–measurement differences. We show that accounting for these two effects—variability in per-particle composition and deviations from the core-shell approximation—reconciles absorption enhancement predictions with laboratory and field observations and resolves the apparent discrepancy. Furthermore, our consistent model framework provides a path forward for improving predictions of BC's radiative effect on climate.

black carbon | direct radiative forcing | absorption enhancement | aerosol mixing state

Black carbon (BC) absorbs solar radiation and has a strong warming effect on climate, estimated as second only to CO_2 (1). However, the scientific understanding of the factors that drive variability in the light absorption per BC mass remains inadequate and contributes to the large uncertainty in BC climate forcing. Light absorption by unmixed BC is reasonably well characterized (2–4), but internal mixing between BC and other aerosol components through processes such as gas condensation and coagulation can enhance the absorption by BC (4–7). The impact of internal mixing is not well understood, with disparities between laboratory observations and field studies (8). Laboratory studies typically show strong enhancement in BC light absorption, often by a factor of two or more for sufficiently large coating amounts (6, 9). However, absorption enhancements by ambient BC vary among field studies, with several studies showing much weaker absorption enhancement for similar average coating amounts (8, 10, 11). Related, primary particles produced from biomass combustion similarly exhibit small absorption enhancements despite large average coating amounts (5). These differences in absorption enhancement between laboratory and field studies suggest that 1) BC-containing particles found in the atmosphere differ from laboratory BC-containing particles in some critical way and 2) variability in the processes that control aerosol mixing—from emission to deposition—plays a key role in establishing absorption enhancements. This laboratory-ambient discrepancy translates into ambiguity in model representations of absorption by BC-containing particles and, thereby, uncertainty in model predictions of atmospheric warming by BC.

BC in the atmosphere is distributed among complex particles of varied size, shape, and chemical composition. However, atmospheric models necessarily approximate the full complexity and diversity of BC-containing particle composition and internal morphology, which we show affects model predictions of the

Significance

Absorption by black carbon strongly affects regional and global climate. Yet, large discrepancies between standard model predictions and regionally specific observations—often with observed absorption lower than expected—raise questions about current understanding of black carbon absorption and its atmospheric impacts. Through a combination of measurement and modeling, our analysis resolves the discrepancy by showing that particular laboratory designs or atmospheric conditions engender distinct compositional heterogeneity among particles containing black carbon. Lower-than-expected absorption results largely from increased heterogeneity, although slightly lowered absorption occurs even in a purely homogeneous system. This work provides a framework that explains globally disparate observations and that can be used to improve estimates of black carbon's global impact.

Author contributions: L.F., T.B.O., and C.D.C. designed research; L.F., T.B.O., C.D.C., C.M., S.C., J.B., P.D., D.A.F., T.H., A.T.L., A.J.S., G.D.S., and L.W. performed research; L.F. analyzed data; and L.F., T.B.O., C.D.C., and C.M. wrote the paper.

The authors declare no competing interest.

This article is a PNAS Direct Submission.

Data deposition: The input files for the PartMC-MOSAIC simulations, the field and laboratory data shown in the figures, and the Python script used to analyze data and make figures are available in GitHub, https://github.com/lfierce2/fierce2020_BC-abs-mixing.

[1]To whom correspondence may be addressed. Email: lfierce@bnl.gov.

[2]Present address: Department of Chemistry and Physics, Western Carolina University, Cullowhee, NC 28723.

[3]Present address: Air Quality Planning and Science Division, California Air Resources Board, Sacramento, CA 95814.

First published February 25, 2020.

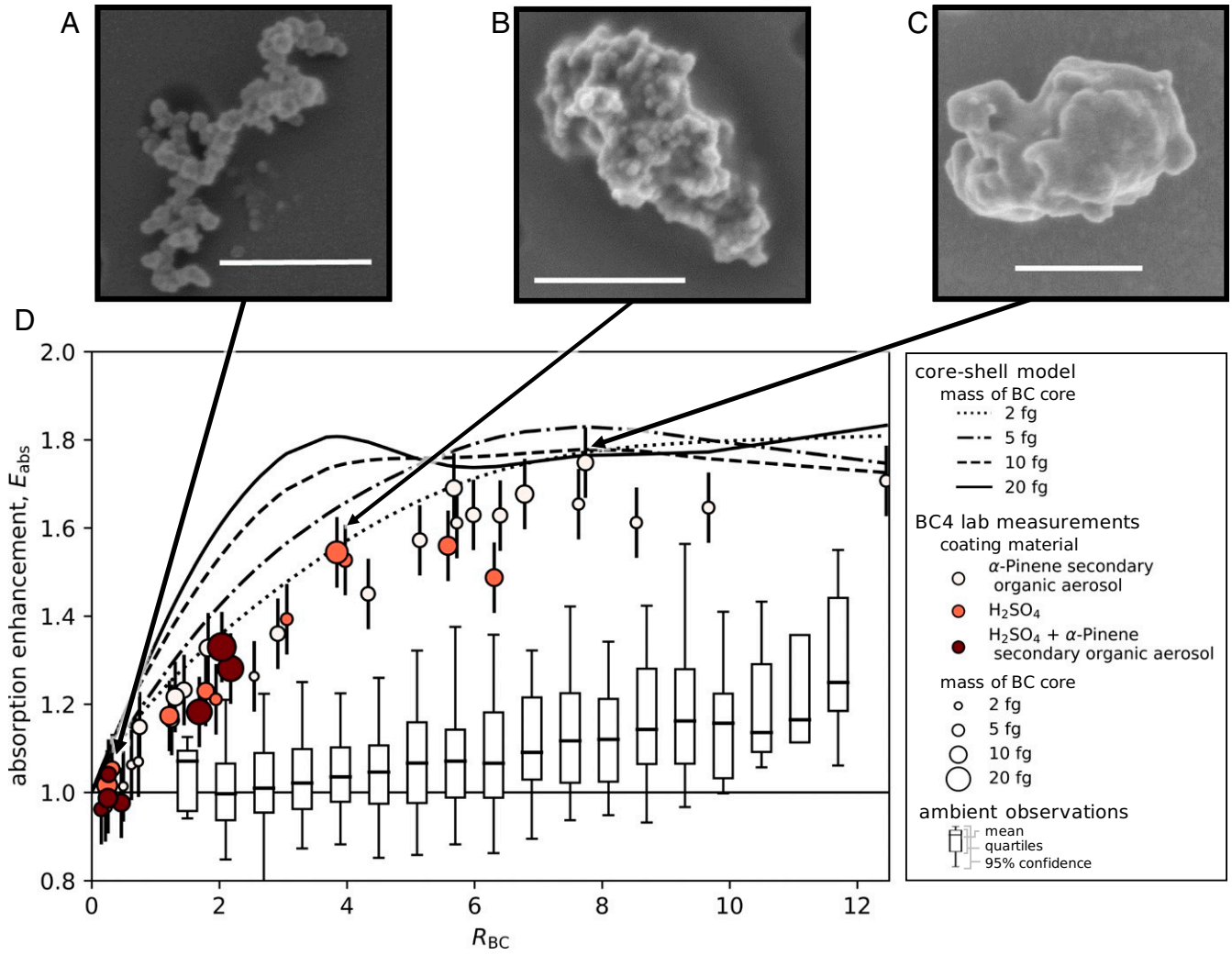

Fig. 1. The complex, noncore-shell morphology of BC-containing particles (*A–C*) leads to lower enhancements in light absorption (denoted E_{abs}; circles in *D*) than predicted under the core-shell approximation (black lines in *D*) for a given R_{BC}, consistent with findings reported in refs. 6, 7, and 34. However, both the core-shell model and the measurements from the BC4 experiment predict larger E_{abs} for the same R_{BC} than has been observed in ambient populations (shown by boxes in *D*) for BC sampled in urban outflow near Fontana, CA (10). The R_{BC} values for the ambient measurements are ensemble averages. The BC4 measurements provide E_{abs} for mass-selected BC cores, where the mass of the BC core, amount of coating, and composition of the coating varied between experiments. Particles were also imaged periodically to capture the internal morphology of the laboratory-generated particles (*A–C*). The model calculations and measurements shown here were performed at a wavelength of 532 nm. (Scale bars: *A–C*, 300 nm.)

associated absorption, typically leading to overestimates. First, while ambient BC exists as a fractal-like structure that may be embedded within or attached to other aerosol components in a variety of ways (12–16) (Fig. 1 *A–C*), BC is typically approximated in models as a spherical core surrounded by a uniform coating, referred to as the core-shell approximation. This core-shell approximation yields greater enhancements in per-particle absorption with the accumulation of coating material than for calculations using more realistic treatments of particle internal morphology (7, 15, 17, 18). Here, we experimentally establish that the core-shell approximation indeed overestimates BC absorption and develop a robust, empirical correction for use in models. Second, and of particular importance, is how the distribution of BC and non-BC material across the particle population is treated. Ambient BC is distributed among diverse particles of varied composition (19, 20). Models, however, often apply the simplifying approximation that particles within the same population or class contain identical mass fractions of constituent aerosol species (21–24), which we refer to as the uniform composition approximation. Previous studies using the Particle Monte Carlo Model for Simulating Aerosol Interactions and Chemistry (PartMC-MOSAIC) have suggested that this uniform composition approximation artificially redistributes the coating material relative to the true, heterogeneous population and leads to an overestimation in modeled absorption enhancements (25–27). In this study, we extend the particle-resolved modeling with PartMC-MOSAIC from ref. 26 using an experimentally determined parameterization for per-particle absorption enhancement and apply a Bayesian framework to estimate absorption enhancements under different model assumptions. We show that, by representing both heterogeneity in per-particle composition and deviations from the core-shell approximation, the improved model reconciles the disparity between modeled and observed light absorption enhancements.

Inadequacy of the Core-Shell Approximation

Potential biases in modeled absorption enhancement (denoted E_{abs}) as a result of the core-shell approximation were

investigated through laboratory measurements from the fourth Boston College (BC4) BC experiment (*Methods*) (28). The BC4 measurements provide a process-level understanding of the response in BC absorption to internal mixing, made possible through improved methods for generating realistically complex primary BC particles and for mixing the BC with other aerosol components (e.g., secondary organic aerosol and sulfuric acid coatings). The observed enhancement for size- and mass-selected particles tends to increase with the volume ratio of non-BC components relative to BC (denoted R_{BC}), but the increase at a given R_{BC} is less than predicted using the core-shell approximation, especially when particles have relatively thin coatings (Fig. 1*D*). Corresponding electron microscope images reveal that, for particles containing very little coating, the non-BC components tend to accumulate in voids within the fractal BC structure and are, therefore, unlikely to strongly enhance BC absorption. After all voids in the fractal BC particles are filled by non-BC material, which occurs at $R_{\mathrm{BC}} \approx 1$, the non-BC material continues to accumulate on the surface of the particle and can lead to compaction of the initially fractal-like BC core depending on the coating material properties (e.g., surface tension) and amount (4, 14, 29), shown through comparison between Fig. 1 *A* and *B*. Our observations show that continued accumulation of non-BC material coincident with the collapse of the BC core engenders an increase in absorption, although the enhancement remains lower than predicted by the core-shell approximation (Fig. 1*D*). To account for these morphological effects on absorption cross-sections, we developed an empirical parameterization based on the BC4 data that can be applied to models that use the core-shell approximation (Eqs. **1** and **2** in *Methods*). The degree of disagreement between the core-shell model and the BC4 measurements shows some variation with BC core size, although these differences are typically within the $\approx 8\%$ uncertainty range of the measurements. We found that per-particle absorption enhancements are accurately represented using the relationship in Eqs. **1** and **2**, which depends only on per-particle R_{BC}.

Although the BC4 measurements, consistent with previous laboratory studies (6, 7), indicate that inadequacies of the core-shell approximation contribute to the overestimation in modeled E_{abs}, the BC4 measurements also show larger E_{abs} than is often reported in field observations (box and whisker plot in Fig. 1*D*) (10). Thus, the differences in per-particle E_{abs} between the core-shell model and BC4 measurements are insufficient to explain the gap between the often large E_{abs} predicted by atmospheric models and the much weaker levels of E_{abs} observed in the atmosphere, even for populations with large R_{BC}.

Importance of Compositional Heterogeneity

Enhancements in light absorption by a population of BC-containing particles depend not only on the response of per-particle absorption to the accumulation of coatings but, also, on the particle-to-particle variation in coating amount. The expected dependence of $E_{\mathrm{abs,bulk}}$ on the population-averaged $R_{\mathrm{BC,bulk}}$ for realistically diverse populations was estimated from ensembles of simulations with the particle-resolved model PartMC-MOSAIC (30, 31) following the approach described in ref. 26. The simulations were not designed to reproduce any specific location or event but, rather, to explore the relationship between $E_{\mathrm{abs,bulk}}$ and $R_{\mathrm{BC,bulk}}$ across a wide variety of conditions relevant for urban atmospheres and their outflow. We note that our simulations do not account for all processes that might affect BC-containing particle composition, such as cloud or fog processing, which may have impacted observations in other locations. Nonetheless, the particle-resolved model simulations reveal substantial variability in per-particle R_{BC} resulting from particle emissions from diverse sources and, more importantly, from condensation and coagulation processes by which particles accumulate coating. This heterogeneity is typically not accounted for in atmospheric models, which instead assume uniform composition or, in other words, that all particles within the same population or class contain identical mass fractions of constituent aerosol species.

By accounting for heterogeneity among BC-containing particles along with deviations from the core-shell approximation, our modeling framework reconciles the previously reported gap between modeled and observed $E_{\mathrm{abs,bulk}}$ (Fig. 2*A*). For diverse particle populations, such as those considered here, most of the coating material tends to be mixed with particles containing the smallest amounts of BC mass (25, 26, 32), an effect resulting from the size dependence of the condensation and coagulation processes by which BC accumulates coatings. For a population of differently sized BC cores, the uniform composition approximation leads to an artificial, unrealistic redistribution of coating material from the particles containing small BC cores onto particles containing large BC cores. Importantly, because the particles containing large amounts of BC mass dominate absorption, the redistribution in coating material resulting from the uniform composition approximation leads to overestimation in overall absorption enhancement by populations of BC-containing particles. This is true whether or not deviations from the core-shell approximation are considered.

The ability of the improved model framework to resolve the model–measurement discrepancy is demonstrated by comparing the model predictions with observations of $E_{\mathrm{abs,bulk}}$ across a wide range of $R_{\mathrm{BC,bulk}}$ values for particles sampled near Los Angeles in Fontana, CA, in summer 2015 (10) (*Methods*). We find general consistency between the improved model predictions and the observations. Specifically, both the modeled and observed $E_{\mathrm{abs,bulk}}$ exhibit little increase with $R_{\mathrm{BC,bulk}}$ up to quite large $R_{\mathrm{BC,bulk}}$ values, although the model does still slightly overestimate the observations. This could be due to the fact that the model scenarios are not specifically designed for this region, which is strongly influenced by local emissions that likely further enhance diversity in R_{BC}. Nonetheless, the model–measurement agreement suggests that the mixture of fresh and aged BC in this urban outflow leads to wide variability in per-particle R_{BC}, resulting in relatively small observable $E_{\mathrm{abs,bulk}}$. If only the particle heterogeneity is accounted for and not the deviation from the core-shell approximation at per-particle $R_{\mathrm{BC}} < 4$, the population-averaged $E_{\mathrm{abs,bulk}}$ is still lower than the uniform composition model but notably higher than the model that includes both. Alternatively, if BC is modeled to represent deviations from the core-shell approximation only, without accounting for variability in composition, $E_{\mathrm{abs,bulk}}$ is substantially overestimated (red shading in Fig. 2*A*), especially at large $R_{\mathrm{BC,bulk}}$. This demonstrates that the uniform composition approximation rather than the core-shell approximation prevails as the dominant cause of the previously reported disagreement between modeled and observed $E_{\mathrm{abs,bulk}}$. However, deviations from the core-shell approximation must also be represented, especially for smaller population-averaged $R_{\mathrm{BC,bulk}}$, for accurate representation of absorption by ambient BC (Fig. 2*B*).

Reconciling Disparate Absorption Enhancement Measurements

We generalize the above findings by calculating $E_{\mathrm{abs,bulk}}$ values for multiple, distinct particle ensembles having the same $R_{\mathrm{BC,bulk}}$ but with differences in the extent of particle heterogeneity, from which the overall averages in Fig. 2*A* were determined. While the average modeled $E_{\mathrm{abs,bulk}}$ agree reasonably well with the observations of BC in urban outflow, some individual populations have substantially larger $E_{\mathrm{abs,bulk}}$ or smaller $E_{\mathrm{abs,bulk}}$ than the average. We find that the spread

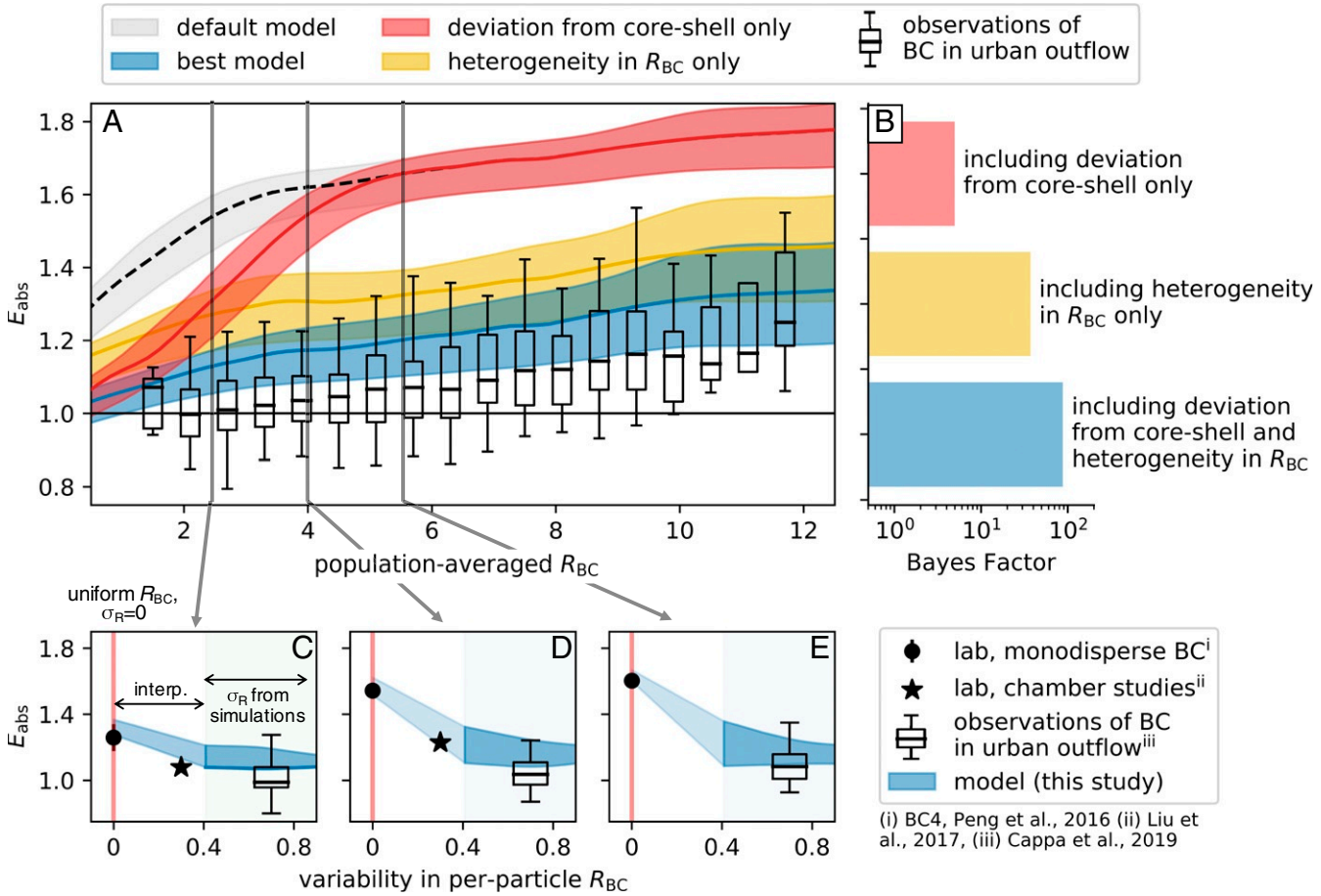

Fig. 2. The previously reported gap between modeled and observed $E_{abs,bulk}$ (illustrated here by comparison of the dashed black line with the box plot in *A*) is largely reconciled by the improved model (blue line and shading in *A*), which accounts for both heterogeneity in R_{BC} and deviations from the core-shell approximation. This improved model is compared with the default model (black line), which assumes a core-shell configuration and neglects particle-to-particle diversity entirely. Evaluation of two additional cases in which only deviation from the core-shell approximation is considered (red shading in *A* and *B*) and in which only heterogeneity in composition is considered (yellow shading in *A* and *B*) shows that neglecting variability in per-particle R_{BC} is the primary cause of differences in modeled and observed $E_{abs,bulk}$. Differences in $E_{abs,bulk}$ between different particle populations having the same $R_{BC,bulk}$—both calculated and observed—are explained by differences in the variability in per-particle R_{BC} (*C*–*E*) between populations. Populations having large variability in per-particle R_{BC}, as expected among ambient BC, are predicted to have weaker levels of $E_{abs,bulk}$ than populations having lower variability in per-particle R_{BC}. Variability in R_{BC} was estimated by fitting the ambient distributions in R_{BC} reported in ref. 7. In all cases, the best estimate (lines) and 1 – σ bounds (shading) were determined from a Bayesian regression of the particle-resolved model data, and the observational strength of one model over another is quantified using the Bayes factor (*Methods*). The measurements and model calculations shown here were performed at a wavelength of 532 nm.

in modeled $E_{\mathrm{abs,bulk}}$ between individual populations at a given $R_{\mathrm{BC,bulk}}$ is largely explained by the extent to which the particles in the population are more or less similar (Fig. 2 *C*–*E*)—greater heterogeneity results in smaller absorption enhancement. The variability within a population is quantified here as the standard deviation (SD) of the logarithm of per-particle R_{BC}, denoted σ_R. (The uniform composition approximation corresponds to $\sigma_R = 0$ or no particle-to-particle variability in R_{BC}.) At a given $R_{\mathrm{BC,bulk}}$, the $E_{\mathrm{abs,bulk}}$ tends to increase as σ_R decreases, reaching a maximum at $\sigma_R = 0$ (Fig. 2 *C*–*E*). The impact of particle heterogeneity generally increases with the overall amount of coating material, with larger differences in $E_{\mathrm{abs,bulk}}$ between $\sigma_R = 0$ and $\sigma_R = 1$ (or larger) when $R_{\mathrm{BC,bulk}}$ is large. These results demonstrate that the observable $E_{\mathrm{abs,bulk}}$ can differ even for the same population-averaged $R_{\mathrm{BC,bulk}}$ depending on the underlying distribution in per-particle R_{BC}. Variability in per-particle R_{BC} will depend on the BC source and the nature of the chemical processing that the particles have undergone. This finding can help to explain differences in measured $E_{\mathrm{abs,bulk}}$ reported across studies.

For example, the particle-resolved simulations suggest that BC sampled in urban outflow exhibits tremendous particle-to-particle variability in R_{BC} and thus particularly small $E_{\mathrm{abs,bulk}}$ as urban plumes comprise BC-containing particles that originate from many different sources and that would have undergone varying extents of atmospheric aging. At the other extreme, laboratory experiments that generate, size-select, and coat BC-containing particles aim to minimize σ_{R}. In such cases, $E_{\mathrm{abs,bulk}}$ is well represented by the uniform composition approximation (vertical red lines at $\sigma_R = 0$ in Fig. 2 *C*–*E*). Alternatively, in laboratory studies in which polydisperse BC is coated via condensation, the population of BC-containing particles will exhibit some variability in per-particle R_{BC} ($\sigma_{\mathrm{R}} \approx 0.4$) (7) but likely substantially less than compared with an urban outflow. Thus, the $E_{\mathrm{abs,bulk}}$ measured for coated, polydisperse BC particles is likely elevated compared with ambient measurements in urban environments but lower than in studies using monodisperse particles (e.g., BC4 results reported in this study) (6). To estimate the dependence of $E_{\mathrm{abs,bulk}}$ on σ_R for populations in which σ_R is >0 but smaller than the smallest σ_R in the

particle-resolved ensemble, we interpolated between $E_{\mathrm{abs,bulk}}$ values under the uniform composition approximation ($\sigma_R = 0$) and $E_{\mathrm{abs,bulk}}$ from the particle-resolved simulations ($\sigma_R > 0.5$). These relatively low σ_R values may be relevant for particles undergoing processing in plumes from well-defined sources, such as from some biomass-burning events. However, temporal or spatial variability in properties of the emitted particles would still contribute to enhanced diversity and, thus, lower $E_{\mathrm{abs,bulk}}$ relative to a population with uniform composition. Of additional consideration not directly included here is the impact of long-range transport of extra-urban biomass-burning plumes (33) or the impact of processing through clouds or fogs that might enhance or reduce particle diversity via preferential activation, growth, and scavenging of larger or more hygroscopic BC-containing particles. Independent of the pathway by which particles are processed in the atmosphere, the framework set out here allows for quantitatively understanding the impact of coatings on absorption by BC-containing particles.

Discussion and Conclusion

This study provides a bottom-up modeling framework that reproduces measured absorption enhancements by BC-containing particles across field and laboratory measurements. Previous studies have typically implicated inaccurate representation of particle internal morphology and thus misapplication of the core-shell approximation as the reason for model–measurement differences (7, 15, 17, 34, 35). However, here we demonstrate that neglect of heterogeneity in particle composition is the dominant cause of previously reported discrepancies between models and observations, with failure of the core-shell approximation for less thickly coated BC being a secondary effect. Differences in E_{abs} between laboratory measurements and field observations likely stem from differences in the underlying variability in particle-to-particle composition, quantified as σ_R. Importantly, our findings suggest that accurate representation of BC's radiative effects in large-scale models requires accounting for particle-to-particle diversity, in addition to deviations from the core-shell approximation. Most likely, large-scale models overestimate the BC absorption efficiency as they typically assume that all BC-containing particles in a population have the same composition.

To facilitate comparison with measurements, the analysis presented here focuses on enhancements in BC's light absorption due to dry, nonabsorbing coatings and, therefore, results in relatively small $E_{\mathrm{abs,bulk}}$, while also focusing on simulations of urban atmospheres and their outflow. However, this finding does not imply that it is reasonable to simply exclude enhancements in BC's light absorption from models. Coating distributions and the resulting absorption enhancements for BC from different sources (e.g., wildfires) or different processing mechanisms (e.g., fogs and clouds) remain a topic for future study. Furthermore, to robustly and accurately represent absorption by atmospheric BC, enhancements in absorption due to water uptake and absorbing coatings must also be considered. For example, BC that is coated with hygroscopic material will take up water at high relative humidity, which effectively increases per-particle coatings and thereby, $E_{\mathrm{abs,bulk}}$. Levels of $E_{\mathrm{abs,bulk}}$ for BC at ambient relative humidity are likely larger than those reported here and likely depend on particle-to-particle variability in the coating's hygroscopicity and refractive index, in addition to the strong dependence on variability in coating amount shown here. This may help to explain why ref. 1 reported that some level of absorption enhancement, 50% on average, is required to reproduce measured BC absorption. As tracking particle-to-particle heterogeneity within particle populations is computationally impractical for current global climate models, the impact of particle diversity must be represented by parameterizing the effect of the unresolved particle characteristics (26) or by finding efficient ways to represent aerosol size–composition distributions (36, 37). The findings presented here suggest that enhancements in BC's light absorption due to internal mixing cannot be ignored, but quantifying the impact of internal mixing will require measurements and models that adequately represent the true complexity of the aerosol mixing state.

Methods

BC4 Experiments. The BC4 experiments quantified the dependence of absorption on coating amount for size-selected BC mass with uniform coating, which is used to derive the relationship between per-particle E_{abs} and per-particle R_{BC}. Particles of BC were generated from an inverted methane codiffusion flame. The polydisperse particles were coated to varying amounts with four coating types: 1) secondary organic aerosol produced from the reaction of α-pinene + OH; 2) secondary organic aerosol produced from the naphthalene + OH reaction, which is somewhat absorbing at 405 nm; 3) H_2SO_4 produced from the SO_2 + OH reaction; and 4) a mixture of α-pinene secondary organic aerosol and H_2SO_4. The coating reactions occurred in a potential aerosol mass (PAM) reactor (38). Polydisperse-coated particles were first selected according to their electrical mobility diameters (using a differential mobility analyzer) and then by their per-particle mass (using a centrifugal particle mass analyzer). By adjusting the PAM reaction conditions and selecting particular combinations of coated particle mass and coated particle mobility diameter, a wide range of coating thicknesses could be attained for particular BC core sizes. BC core volume-equivalent diameters ranged from 93 to 284 nm, with most measurements around the experiment average of 173 nm. Measured coating-to-core mass ratios were converted to coating-to-core volume ratios accounting for density differences between the core (BC = 1.8 g cm^{-3}) and the coatings (secondary organic aerosol [SOA] = 1.3 g cm^{-3} and H_2SO_4 = 1.8 g cm^{-3}). The absorption by the monodisperse particles was measured using the University of California Davis photoacoustic spectrometer (UCD-PAS) (8, 39) at 532 nm (and 405 nm); complementary measurements were made at other wavelengths with the University of Georgia four-wavelength photoacoustic system (406, 532, 662, and 785 nm) (40) and the Aerodyne single-scattering albedo monitor (630 nm) (41) and yield consistent results. Absorption was measured for both coated and uncoated particles, with the latter generated by passing the monodisperse particles through a thermodenuder to remove the non-BC coating material. Particle composition measurements made using an aerosol mass spectrometer confirmed that the coating material was completely removed and established the relative composition for the mixed coating experiments. The absorption enhancement was determined as the ratio between the coated and uncoated (thermally denuded) particle absorption corrected for losses in the thermodenuder and for the influence of multiply charged particles (42). Further details are available in refs. 42 and 43.

Empirical Relationship for Per-Particle E_{abs}. As discussed in the text, comparison between E_{abs} from the BC4 measurements (circles in Fig. 1*D*) and for the same volume-equivalent BC core diameter, $E_{\mathrm{abs,cs}}$ from the core-shell model (black lines in Fig. 1*D*) shows that the core-shell model overestimates the observed E_{abs} for thinly coated particles but, for thickly coated particles, predicts enhancements similar to the laboratory measurements. To account for this deviation from the core-shell approximation in the particle-resolved simulations, we derived an empirical parameterization for per-particle absorption enhancement, which is represented as a central estimate E_{abs} and an error term ϵ:

$$E_{\mathrm{abs}} = 1 + \frac{R_{\mathrm{BC}}}{R_{\mathrm{BC,0}}}(E_{\mathrm{abs,cs}} - 1) + \epsilon \qquad R_{\mathrm{BC}} < R_{\mathrm{BC,0}} \qquad [1]$$

$$E_{\mathrm{abs}} = E_{\mathrm{abs,cs}} + \epsilon \qquad R_{\mathrm{BC}} \geq R_{\mathrm{BC,0}}. \qquad [2]$$

Similar in form to the parameterization given in equations 4 and 5 of ref. 7, the central estimate for E_{abs} is expressed as a weighted average between $E_{\mathrm{abs,cs}}$, the absorption enhancement from the core-shell approximation, and $E_{\mathrm{abs}} = 1$, corresponding to no enhancement, until particles reach some threshold amount of coating denoted $R_{\mathrm{BC,0}}$, which is a constant. The parameterized E_{abs} is more heavily weighted toward $E_{\mathrm{abs}} = 1$ for small R_{BC} and is more heavily weighted toward $E_{\mathrm{abs}} = E_{\mathrm{abs,cs}}$ as R_{BC} approaches $R_{\mathrm{BC,0}}$. After R_{BC} exceeds a threshold $R_{\mathrm{BC,0}}$, it is assumed that $E_{\mathrm{abs}} = E_{\mathrm{abs,cs}}$. The error term ϵ is a normal distribution with SD σ_E, where σ_E is assumed to be constant across all coating-to-BC ratios R_{BC}.

We applied a Bayesian approach to find the expected value of the parameter set $\vec{\theta} = [R_{BC,0}, \sigma_E]$ using laboratory experiments in which per-particle BC mass, coating mass, and coating composition were varied, and absorption was measured at three different wavelengths (405, 532, and 632 nm). We spanned combinations of parameters within the range $0 < R_{BC,0} < 20$ and $0.001 < \epsilon < 1$, where the space describing the sampled prior distribution is defined by hyperparameter α, and predicted the posterior probability of each parameter combination m given the BC4 measurement dataset **X**:

$$p(\vec{\theta}_m \mid \mathbf{X}, \alpha) = \frac{p(\mathbf{X} \mid \vec{\theta}_m, \alpha)}{\sum_m p(\mathbf{X} \mid \vec{\theta}_m, \alpha) p(\vec{\theta}_m \mid \alpha)} p(\vec{\theta}_m \mid \alpha)$$
$$= \frac{\prod_i p(E_{abs} \mid R_{BC}, \vec{\theta}_m, \alpha)}{\sum_m \prod_i p(E_{abs} \mid R_{BC}, \vec{\theta}_m, \alpha) p(\vec{\theta}_m \mid \alpha)} p(\vec{\theta}_m \mid \alpha). \quad [3]$$

The expected value of $\theta = [R_{BC,0}, \sigma_E]$ was then computed as the average of each parameter combination θ_m weighted by the posterior probability $p(\vec{\theta}_m \mid \mathbf{X}, \alpha)$:

$$E[\vec{\theta} \mid \mathbf{X}, \alpha] = \sum_m \vec{\theta}_m p(\vec{\theta}_m \mid \mathbf{X}, \alpha). \quad [4]$$

We found a threshold of $R_{BC,0} = 4.1$ and an SD of $\sigma_E = 0.1$. The parameterization given in Eqs. **1** and **2** with these coefficients accurately reproduces the BC4 laboratory measurements independent of wavelength. Only results at 532 nm are presented in the text. All core-shell model calculations in this study were performed using PyMieScatt (44). The parameterization in Eqs. **1** and **2** is suitable for any model using the core-shell approximation, including reduced aerosol schemes used in global models. However, as we have shown in the main text, application of this parameterization for per-particle absorption is not sufficient to improve modeled absorption; models must also account for particle-to-particle heterogeneity in R_{BC}.

Predicting $E_{abs,bulk}$ from Particle-Resolved Model. The population-level $E_{abs,bulk}$ for realistically diverse particle populations was estimated from simulations with PartMC-MOSAIC (30, 31). PartMC-MOSAIC simulates the aerosol evolution due to primary particle emissions, condensation and evaporation of semivolatile gases, coagulation between particles, and dilution with background air. The high-dimensional aerosol size–composition distribution is modeled in PartMC by tracking 5,000 to 100,000 Monte Carlo particles. MOSAIC simulates gas- and aerosol-phase chemistry, and secondary organic aerosol formation is simulated in MOSAIC using the SORGAM scheme (45). All aerosol species relevant for urban atmospheres are simulated, including SO_4^{2-}, NO_3^-, NH_4^+, Na^+, Ca^{2+}, other inorganic mass (including species such as SiO_2, metal oxides, and other unmeasured or unknown inorganic species present in aerosols), BC, primary organic carbon, secondary organic carbon, and water. In contrast to aerosol schemes in large-scale models, which necessarily simplify the representation of particle size and composition, PartMC-MOSAIC resolves the full dimensionality of the aerosol mixing state and can, therefore, be viewed as a benchmark scheme for evaluating approximate representations of particle physical and chemical properties. PartMC version 2.1.5 was used for the simulations in this study and is available at http://lagrange.mechse.illinois.edu/partmc/. MOSAIC is available on request from Rahul A. Zaveri, Pacific Northwest National Laboratory, Richland, WA.

The absorption enhancement $E_{abs,bulk}$ for a population of BC-containing particles is the ratio between the population-averaged absorption coefficient for the internally mixed BC, b_{abs}, and the absorption coefficient by the same population if all BC was uncoated, $b_{abs,uncoated}$, where the coated and uncoated absorption coefficients are the sum over the particles' respective absorption cross-sections per volume of air that the particles occupy. Applying the assumption that the mass absorption coefficient (MAC) for uncoated BC is a constant at each wavelength, independent of BC core size, the overall $E_{abs,bulk}$ is estimated as the average across per-particle $E_{abs,i}$ for each BC-containing $i = 1, \ldots, N_{BC}$, weighted by the per-particle BC mass $m_{BC,i}$:

$$E_{abs,bulk} = \frac{\sum_i^{N_{BC}} E_{abs,i} m_{BC,i}}{\sum_i^{N_{BC}} m_{BC,i}}. \quad [5]$$

The per-particle absorption enhancement is computed for each of the thousands of particles simulated by PartMC-MOSAIC using either the core-shell approximation or the empirical parameterization given in Eqs. **1** and **2**. At each model time step, PartMC-MOSAIC provides the mass of each aerosol species contained in each particle. Taking as inputs the volume-equivalent diameter of the BC core, the volume or thickness of the coating, and the wavelength-dependent refractive indices for the BC core and coating, the absorption enhancement under the core-shell approximation, $E_{abs,cs}$, is predicted as the ratio between the absorption cross-section of a spherical BC core having a uniform coating thickness and the absorption cross-section of an uncoated BC core. The parameterization in Eqs. **1** and **2** then predicts the adjusted E_{abs} as a function of $E_{abs,cs}$ and R_{BC}. The volume-equivalent BC core diameter is computed from the per-particle BC mass from PartMC-MOSAIC, assuming that the density of BC is 1.8 g cm^{-3}. The thickness of the shell is computed from the mass of the non-BC components, with the assumed density for each aerosol species listed in table 1 of the supplemental information of ref. 26. In this study, water is excluded from the shell material for optical calculations for consistency with field and laboratory measurement of, typically, dry aerosol. The refractive index of the shell material is computed as the volume-weighted average of the refractive indices of non-BC components, where the assumed refractive index for each aerosol component is provided in table 1 of the supplemental information of ref. 26.

In order to assess the impact of the uniform composition approximation, we compared the enhancements from the particle-resolved simulations, E_{abs}, with enhancements computed under the uniform composition approximation, $\tilde{E}_{abs}$. We assume that the mass of BC contained in each particle is the same under the uniform composition approximation as simulated by the particle-resolved model, and the mass of every other component, $\tilde{m}_{a,i}$, is adjusted such that the ratio between species a and BC in each particle i is the same as the ratio between the total mass of species a contained in all BC-containing particles and the total mass of BC:

$$\tilde{m}_{a,i} = m_{BC,i} \frac{\sum_i m_{a,i}}{\sum_i m_{BC,i}}. \quad [6]$$

Ensembles of Urban Scenarios. To quantify the general dependence of $E_{abs,bulk}$ on $R_{BC,bulk}$ expected in urban atmospheres, we analyzed populations of BC-containing particles sampled from an ensemble of 100 PartMC-MOSAIC simulations. The input parameters were varied across the 100 scenarios to represent populations of BC-containing particles that had aged to varying degrees under the wide range of conditions expected in urban atmospheres and their outflow. While the specific settings differed among simulations, the general setup was the same. In each case, the model tracks the composition of ~5,000 particles in a well-mixed air parcel, which is meant to represent a slice of the well-mixed boundary layer during the first 12 h of simulation and a slice of the residual layer thereafter. All simulations started at 6:00 AM, at which time the parcel contained only background gas and aerosol. In each simulation, the parcel received emissions of gases and primary aerosol from 6:00 AM until 6:00 PM each day. Input parameters for each of the 100 scenarios were sampled from a 30-dimensional parameter space using Latin Hypercube sampling, yielding scenarios that span a wide range of meteorological conditions, gas and aerosol emission rates, size distribution parameters for background and emitted aerosol, and composition for background and emitted aerosol. The range over which input parameters are varied to generate the ensemble of 100 scenarios is given in supplementary table 3 of ref. 26.

Conditional Probability of $E_{abs,bulk}$ Given $R_{BC,bulk}$. For a known $R_{BC,bulk}$, the population-averaged absorption enhancement $E_{abs,bulk}$ is represented by a probability density distribution rather than a single value because populations having the same $R_{BC,bulk}$ may yield very different levels of absorption enhancement depending on the underlying size–composition distribution. For each set of model assumptions M_k for $k = 1, \ldots, 4$ (Table 1), we determined the conditional probability of $E_{abs,bulk}$ given the population-averaged $R_{BC,bulk}$:

$$p(E_{abs} \mid R_{BC}, M_k) = \frac{p(R_{BC,bulk}, E_{abs,bulk} \mid M_k)}{p(R_{BC,bulk})}. \quad [7]$$

Table 1. Model assumptions explored in this study

Model	Description of assumptions
M_1	Default: core-shell approximation, uniform composition approximation
M_2	Including deviation from core shell only while assuming uniform composition
M_3	Including heterogeneity in R_{BC} only while assuming core shell
M_4	Including deviation from core shell and heterogeneity in R_{BC}

The univariate and bivariate density functions, $p(R_{BC,bulk})$ and $p(R_{BC,bulk}, E_{abs,bulk} \mid M_k)$, respectively, are computed using kernel density estimation (46, 47). The value of the univariate density function at some target $R_{BC,bulk}$, $p(R_{BC,bulk})$, is estimated from the sum over all simulated populations weighted by a kernel function that depends on the difference between the population-averaged $R_{BC,bulk,j}$ for each population $j = 1, \ldots, N_{populations}$ and the target R_{BC}. Here, we assume a Gaussian kernel function, $K_R\left((R_{BC,bulk} - R_{BC,bulk,j})^2\right)$, such that populations with $R_{BC,bulk,j}$ near the target are heavily weighted, yielding a smooth approximation of $p(R_{BC,bulk})$ for the ensemble of scenarios:

$$p(R_{BC,bulk}) = \sum_j K_R\left((R_{BC,bulk} - R_{BC,bulk,j})^2\right). \quad [8]$$

Similarly, the bivariate density function, $p(R_{BC,bulk}, E_{abs,bulk} \mid M_k)$, is computed using bivariate kernel density estimation, where $K_R((R_{BC,bulk} - R_{BC,bulk,j})^2)$ is again the kernel-weighting function with respect to $R_{BC,bulk}$, and $K_E((E_{abs,bulk} - E_{abs,bulk,j})^2)$ is the kernel-weighting function with respect to $E_{abs,bulk}$. However, when modeled using the empirical parameterization, population-averaged absorption enhancement for each population is not represented by a single value but, rather, by a normal distribution with mean and variance predicted by the parameterization. The variance in the absorption enhancement is represented using 5-point Gauss–Hermite quadrature such that absorption enhancement at each time step j is represented by quadrature points $E_{abs,j,q}$ and w_q for $q = 1, \ldots, 5$. The quadrature points and weights are then incorporated into the kernel density estimation:

$$p(R_{BC,bulk}, E_{abs,bulk} \mid M_k) = \sum_j K_R\left((R_{BC,bulk} - R_{BC,bulk,j})^2\right) \times \sum_q w_q K_E\left((E_{abs,bulk} - E_{abs,bulk,j,q})^2\right). \quad [9]$$

For the most realistic model approximation, M_4, which represents the true diversity in composition for each particle-resolved population and applies the laboratory-based parameterization for per-particle E_{abs}, we extend the approach to estimate the conditional probability of $E_{abs,bulk}$ given two parameters, the population-averaged $R_{BC,bulk}$ and a metric of variance in per-particle R_{BC}, quantified here as the SD of the logarithm of per-particle R_{BC} and denoted σ_R:

$$p(E_{abs,bulk} \mid R_{BC,bulk}, \sigma_R) = \frac{p(R_{BC,bulk}, \sigma_R \mid E_{abs,bulk}) p(E_{abs,bulk})}{p(R_{BC,bulk}, \sigma_R)} = \frac{p(R_{BC,bulk}, \sigma_R, E_{abs,bulk})}{p(R_{BC,bulk}, \sigma_R)}. \quad [10]$$

The trivariate density function $p(R_{BC,bulk}, \sigma_R, E_{abs,bulk})$ and bivarite density function $p(R_{BC,bulk}, \sigma_R)$ are computed using the kernel density estimation. Each kernel function requires a bandwidth, and the resulting probability density function is sensitive to the assumed bandwidth. As in ref. 26, the bandwidth for each variable was selected using Silverman's rule of thumb (48).

Observations of E_{abs} by BC in Urban Outflow. Model predictions of E_{abs} were compared with measurements made in Fontana, CA. The field measurements took place over a 3-wk period in July 2015, with full details provided in ref. 10. Absorption by PM1 (particulate matter with diameter < 1 μm) was measured using the UCD-PAS at 532 nm. The absorption enhancement was determined from measurements of the MAC normalized to the MAC estimated for uncoated BC. The MAC is the ratio between the observed absorption and the measured BC concentration, with the latter determined using a single-particle soot photometer calibrated using fullerene soot. The ensemble average coating-to-core ratio was determined using a soot particle aerosol mass spectrometer (49).

Bayes Factor for Evaluating Models. The strength of the observational evidence in support of one model over another was quantified using the Bayes factor, K. In our case, the Bayes factor quantifies the likelihood given the observational evidence of an improved model, M_k for $k = 2, 3, 4$, over the default model, M_1:

$$K = \frac{p(M_k \mid \text{observations})}{p(M_1 \mid \text{observations})} = \frac{p(\text{observations} \mid M_k) p(M_k)}{p(\text{observations} \mid M_1) p(M_1)} = \frac{\sum_k p(E_{abs,bulk,k} \mid R_{BC,bulk,k}, M_k)}{\sum_k p(E_{abs,bulk,k} \mid R_{BC,bulk,k}, M_1)}. \quad [11]$$

Data Availability. PartMC version 2.1.5 was used for the simulations in this paper, which is available at http://lagrange.mechse.illinois.edu/partmc/. MOSAIC is available from Rahul A. Zaveri. The core-shell optical calculations were performed with PyMieScatt, which is available at https://github.com/bsumlin/PyMieScatt. The input files for the PartMC-MOSAIC simulations, the field and laboratory data shown in the figures, and the Python script used to analyze data and make figures are available at https://github.com/lfierce2/fierce2020_BC-abs-mixing.

ACKNOWLEDGMENTS. We acknowledge all participants of the BC4 laboratory study, including Leah Williams, Jesse Kroll, Ellie Browne, Gabriel Isaacman-Wertz, Yatish Parmar, James Brogan, Sara Forestieri, and Noopur Sharma. Parts of this study were completed using Michigan Technological University's Applied Chemical and Morphological Analysis Laboratory. The BC4 study was supported by US Department of Energy (DOE) Grant DE-SC0011935 and National Science Foundation Grants AGS-1244918 (to Boston College) and AGS-1244999 (to Aerodyne). The participation of the single-particle soot photometer was made possible by a DOE Atmospheric Radiation Measurement Climate Research Facility small campaign grant. S.C. is supported by the Environmental Molecular Sciences Laboratory, a national scientific user facility sponsored by the DOE's Office of Biological and Environmental Research at Pacific Northwest National Laboratory. L.F. was supported under the DOE Atmospheric System Research program at Brookhaven National Laboratory, a multiprogram national laboratory supported by DOE Contract DE-SC0012704.

1. T. C. Bond *et al.*, Bounding the role of black carbon in the climate system: A scientific assessment. *J. Geophys. Res. Atmos.* **118**, 5380–5552 (2013).
2. A. Petzold, M. Schönlinner, Multi-angle absorption photometry—a new method for the measurement of aerosol light absorption and atmospheric black carbon. *J. Aerosol Sci.* **35**, 421–441 (2004).
3. T. C. Bond, R. W. Bergstrom, Light absorption by carbonaceous particles: An investigative review. *Aerosol. Sci. Technol.* **40**, 27–67 (2006).
4. E. S. Cross *et al.*, Soot particle studies—instrument inter-comparison—project overview. *Aerosol. Sci. Technol.* **44**, 592–611 (2010).
5. G. McMeeking *et al.*, Impacts of nonrefractory material on light absorption by aerosols emitted from biomass burning. *J. Geophys. Res. Atmos.* **119**, 12272–12286 (2014).
6. J. Peng *et al.*, Markedly enhanced absorption and direct radiative forcing of black carbon under polluted urban environments. *Proc. Natl. Acad. Sci. U.S.A.* **113**, 4266–4271 (2016).
7. D. Liu *et al.*, Black-carbon absorption enhancement in the atmosphere determined by particle mixing state. *Nat. Geosci.* **10**, 184–188 (2017).
8. C. D. Cappa *et al.*, Radiative absorption enhancements due to the mixing state of atmospheric black carbon. *Science* **337**, 1078–1081 (2012).
9. M. Schnaiter *et al.*, Absorption amplification of black carbon internally mixed with secondary organic aerosol. *J. Geophys. Res.* **110**, D19204 (2005).
10. C. D. Cappa *et al.*, Light absorption by ambient black and brown carbon and its dependence on black carbon coating state for two California, USA cities in winter and summer. *J. Geophys. Res. Atmos.* **124**, 1550–1577 (2019).
11. R. M. Healy *et al.*, Light-absorbing properties of ambient black carbon and brown carbon from fossil fuel and biomass burning sources. *J. Geophys. Res. Atmos.* **120**, 6619–6633 (2015).
12. S. China, C. Mazzoleni, K. Gorkowski, A. C. Aiken, M. K. Dubey, Morphology and mixing state of individual freshly emitted wildfire carbonaceous particles. *Nat. Commun.* **4**, 2122 (2013).
13. N. Sharma *et al.*, Physical properties of aerosol internally mixed with soot particles in a biogenically dominated environment in California. *Geophys. Res. Lett.* **45**, 11473–11482 (2018).
14. R. C. Moffet *et al.*, Morphology and mixing of black carbon particles collected in central California during the cares field study. *Atmos. Chem. Phys.* **16**, 14515–14525 (2016).
15. K. Adachi, S. H. Chung, P. R. Buseck, Shapes of soot aerosol particles and implications for their effects on climate. *J. Geophys. Res.* **115**, D15206 (2010).
16. K. Adachi, N. Moteki, Y. Kondo, Y. Igarashi, Mixing states of light-absorbing particles measured using a transmission electron microscope and a single-particle soot photometer in tokyo, Japan. *J. Geophys. Res. Atmos.* **121**, 9153–9164 (2016).
17. B. Scarnato, S. Vahidinia, D. Richard, T. Kirchstetter, Effects of internal mixing and aggregate morphology on optical properties of black carbon using a discrete dipole approximation model. *Atmos. Chem. Phys.* **13**, 5089–5101 (2013).
18. L. Liu, M. Mishchenko, Scattering and radiative properties of morphologically complex carbonaceous aerosols: A systematic modeling study. *Rem. Sens.* **10**, 1634 (2018).
19. M. Shiraiwa *et al.*, Radiative impact of mixing state of black carbon aerosol in asian outflow. *J. Geophys. Res.* **113**, D24210 (2008).
20. R. M. Healy *et al.*, Single particle diversity and mixing state measurements. *Atmos. Chem. Phys.* **14**, 6289–6299 (2014).
21. P. Stier *et al.*, The aerosol-climate model echam5-ham. *Atmos. Chem. Phys.* **5**, 1125–1156 (2005).

22. S. Bauer *et al.*, Matrix (multiconfiguration aerosol tracker of mixing state): An aerosol microphysical module for global atmospheric models. *Atmos. Chem. Phys.* **8**, 6003–6035 (2008).
23. G. Mann *et al.*, Description and evaluation of glomap-mode: A modal global aerosol microphysics model for the ukca composition-climate model. *Geosci. Model Dev.* **3**, 519–551 (2010).
24. X. Liu *et al.*, Description and evaluation of a new four-mode version of the modal aerosol module (mam4) within version 5.3 of the community atmosphere model. *Geosci. Model Dev.* **9**, 505–522 (2016).
25. R. A. Zaveri, J. C. Barnard, R. C. Easter, N. Riemer, M. West, Particle-resolved simulation of aerosol size, composition, mixing state, and the associated optical and cloud condensation nuclei activation properties in an evolving urban plume. *J. Geophys. Res.* **115**, D17210 (2010).
26. L. Fierce, T. C. Bond, S. E. Bauer, F. Mena, N. Riemer, Black carbon absorption at the global scale is affected by particle-scale diversity in composition. *Nat. Commun.* **7**, 12361 (2016).
27. L. Fierce, N. Riemer, T. C. Bond, Toward reduced representation of mixing state for simulating aerosol effects on climate. *Bull. Am. Meteorol. Soc.* **98**, 971–980 (2017).
28. L. Fierce *et al.*, Measurements, simulations, and processing code for "Radiative absorption enhancements by black carbon controlled by particle-to-particle heterogeneity in composition." GitHub and linked in Zenodo. https://doi.org/10.5072/zenodo.493385. Deposited 10 February 2020.
29. J. Bhandari *et al.*, Extensive soot compaction by cloud processing from laboratory and field observations. *Sci. Rep.* **9**, 1–12 (2019).
30. N. Riemer, M. West, R. A. Zaveri, R. C. Easter, Simulating the evolution of soot mixing state with a particle-resolved aerosol model. *J. Geophys. Res.* **114**, D09202 (2009).
31. R. A. Zaveri, R. C. Easter, J. D. Fast, L. K. Peters, Model for simulating aerosol interactions and chemistry (mosaic). *J. Geophys. Res.* **113**, D13204 (2008).
32. A. Metcalf *et al.*, Black carbon aerosol over the Los Angeles basin during CalNex. *J. Geophys. Res. Atmos.* **117**, D00V13 (2012).
33. S. Liu *et al.*, Enhanced light absorption by mixed source black and brown carbon particles in UK winter. *Nat. Commun.* **6**, 8435 (2015).
34. R. K. Chakrabarty, W. R. Heinson, Scaling laws for light absorption enhancement due to nonrefractory coating of atmospheric black carbon aerosol. *Phys. Rev. Lett.* **121**, 218701 (2018).
35. Y. Wu *et al.*, Light absorption enhancement of black carbon aerosol constrained by particle morphology. *Environ. Sci. Technol.* **52**, 6912–6919 (2018).
36. R. McGraw, L. Leng, W. Zhu, N. Riemer, M. West, Aerosol dynamics using the quadrature method of moments: Comparing several quadrature schemes with particle-resolved simulation. *J. Phys. Conf.* **125**, 012020 (2008).
37. L. Fierce, R. L. McGraw, Multivariate quadrature for representing cloud condensation nuclei activity of aerosol populations. *J. Geophys. Res. Atmos.* **122**, 9867–9878 (2017).
38. A. Lambe *et al.*, Characterization of aerosol photooxidation flow reactors: Heterogeneous oxidation, secondary organic aerosol formation and cloud condensation nuclei activity measurements. *Atmos. Meas. Tech.* **4**, 445–461 (2011).
39. D. A. Lack *et al.*, Aircraft instrument for comprehensive characterization of aerosol optical properties, part 2: Black and brown carbon absorption and absorption enhancement measured with photo acoustic spectroscopy. *Aerosol Sci. Technol.* **46**, 555–568 (2012).
40. D. A. Fischer, G. D. Smith, A portable, four-wavelength, single-cell photoacoustic spectrometer for ambient aerosol absorption. *Aerosol. Sci. Technol.* **52**, 393–406 (2018).
41. T. B. Onasch *et al.*, Single scattering albedo monitor for airborne particulates. *Aerosol. Sci. Technol.* **49**, 267–279 (2015).
42. S. D. Forestieri *et al.*, Measurement and modeling of the multiwavelength optical properties of uncoated flame-generated soot. *Atmos. Chem. Phys.* **18**, 12141–12159 (2018).
43. T. M. Helgestad, *Characterizing the Optical Properties of Coated Black Carbon Particles* (University of California, Davis, CA, 2016).
44. B. J. Sumlin, W. R. Heinson, R. K. Chakrabarty, Retrieving the aerosol complex refractive index using pymiescatt: A mie computational package with visualization capabilities. *J. Quant. Spectrosc. Radiat. Transf.* **205**, 127–134 (2018).
45. B. Schell, I. J. Ackermann, H. Hass, F. S. Binkowski, A. Ebel, Modeling the formation of secondary organic aerosol within a comprehensive air quality model system. *J. Geophys. Res. Atmos.* **106**, 28275–28293 (2001).
46. E. A. Nadaraya, On estimating regression. *Theor. Probab. Appl.* **9**, 141–142 (1964).
47. G. S. Watson, Smooth regression analysis. *Sankhya Indian J. Stat. Ser. A* **26**, 359–372 (1964).
48. B. W. Silverman, *Density Estimation for Statistics and Data Analysis* (Chapman & Hall, 1986).
49. T. Onasch *et al.*, Soot particle aerosol mass spectrometer: Development, validation, and initial application. *Aerosol. Sci. Technol.* **46**, 804–817 (2012).